~~RESTRICTED~~

RM L51G30

NACA RM L51G30

UNCLASSIFIED

NACA

RESEARCH MEMORANDUM

A COMPARISON OF THE SPANWISE LOADING CALCULATED BY VARIOUS METHODS WITH EXPERIMENTAL LOADINGS OBTAINED ON A 45° SWEPTBACK WING OF ASPECT RATIO 8 AT A REYNOLDS NUMBER OF 4.0×10^6

By William C. Schneider

Langley Aeronautical Laboratory
Langley Field, Va.

NATIONAL ADVISORY COMMITTEE
FOR AERONAUTICS

WASHINGTON

January 29, 1952

UNCLASSIFIED

~~RESTRICTED~~

NATIONAL ADVISORY COMMITTEE FOR AERONAUTICS

RESEARCH MEMORANDUM

A COMPARISON OF THE SPANWISE LOADING CALCULATED BY VARIOUS METHODS WITH EXPERIMENTAL LOADINGS OBTAINED ON A 45° SWEPTBACK WING OF ASPECT RATIO 8 AT A REYNOLDS NUMBER OF 4.0×10^6

By William C. Schneider

SUMMARY

Experimental force and moment data obtained by pressure measurements on a wing of aspect ratio 8.02, 45° sweepback of the quarter-chord line, taper ratio of 0.45, and NACA 63_1A012 airfoil sections have been compared with the calculated loadings obtained by the standard methods proposed by Weissinger, Falkner, and Multhopp, as well as by several variations of these methods. The most accurate shape of the span load distribution was predicted by the standard Multhopp solution. The standard Falkner 6 × 3 solution failed to predict the experimental dip in the span load distribution at the root stations. All methods that predicted a fairly accurate loading shape predicted the lift-curve slope about 8 percent low. Since all of the methods of calculating are based on thin-wing theory, the underestimation of the lift-curve slope is probably attributable to the finite thickness of the wing. On the basis of the present calculations, the Weissinger method, when the number of control points was increased from 7 (the number suggested by Weissinger) to 15, or the Multhopp method, when using at least 15 control points, is a good compromise between accuracy of the results and time required for a solution.

INTRODUCTION

Various methods exist for the calculation of aerodynamic forces on swept wings but only limited experimental corroboration of the different approaches has been made. As early as 1947, a comparison with experiment was made of the various methods available at that time (reference 1), but the comparison was limited to experimental data obtained on wings of low aspect ratio; and, in addition, the experimental load shape was

somewhat inadequately defined by the small number of spanwise stations available. No comparisons have previously been made for wings having both high aspect ratio and large sweep angle.

Experimental data have been obtained in the Langley 19-foot pressure tunnel on a wing of aspect ratio 8.02, 45° sweepback of the quarter-chord line, taper ratio of 0.45, and NACA 63_1A012 airfoil sections parallel to the plane of symmetry. Pressure data were available from 8 spanwise stations, including one at the plane of symmetry. The present paper compares the loadings computed by the second-order lifting-line method of Weissinger (reference 2) and the lifting-surface methods of Falkner (reference 3) and Multhopp (reference 4) with the experimental loading.

The effects of the spanwise number and distribution of control points, the chordwise distribution of control points, the root-section discontinuity, and the chordwise distribution of circulation on the spanwise loading, lift-curve slope, center of pressure, pitching moment, and induced drag are examined and discussed. The applicability of the calculations at high lift coefficients is also investigated. Also presented are spanwise loadings predicted by the rapid approximate methods of Diederich (reference 5) and Jones (reference 6).

SYMBOLS

$\frac{c_l c}{\bar{c}}$ wing loading parameter

$\frac{c_l c}{C_L \bar{c}}$ unit wing loading parameter

c_l section lift coefficient

$$\left(\cos\alpha\int_{L.E.}^{T.E.}\left(S_u - S_l\right)d\left(\frac{x}{c}\right) - \sin\alpha\int_{-\left(\frac{z}{c}\right)_{max}}^{\left(\frac{z}{c}\right)_{max}}\left(S_r - S_f\right)d\left(\frac{z}{c}\right)\right)$$

C_L wing lift coefficient

$$\left(\frac{1}{2}\int_{-1}^{1}\frac{c_l c}{\bar{c}}\,d\eta \quad \text{or} \quad \frac{L}{qS_w}\right)$$

C_m wing pitching-moment coefficient

C_{D_i}	induced-drag coefficient $\left(\frac{1}{2}\int_{-1}^{1}\frac{c_l c}{\bar{c}}\alpha_i \, d\eta\right)$
c	local wing chord
$\bar{c}$	mean wing chord
b	wing span
S_w	wing area
S	pressure coefficient $\left(\frac{H-p}{q}\right)$
H	free-stream total pressure
p	local static pressure
L	lift
q	free-stream dynamic pressure $\left(\frac{1}{2}\rho V^2\right)$
V	free-stream velocity
ρ	density of air
x	chordwise coordinate, positive rearward
y	spanwise coordinate, positive right
z	normal coordinate, positive up
η	nondimensional spanwise coordinate $\left(\frac{y}{b/2}\right)$
$\bar{y}$	longitudinal coordinate of center of pressure
$\bar{x}$	lateral coordinate of center of pressure along mean aerodynamic chord
C_{L_α}	lift-curve slope, per degree

[redacted]

θ angular chordwise coordinate $\left(\cos^{-1}\left(1 - \frac{x}{c/2}\right)\right)$

$\frac{\Delta v_a}{V}$ ratio of increment of local velocity caused by additional type of load distribution to free-stream velocity

$a_0, a_1, \ldots a_{12}$ coefficients of terms in Fourier representation of chordwise loading

α geometric angle of attack

α_i induced angle of attack

Subscripts:

u upper surface

l lower surface

f forward of maximum thickness

r rearward of maximum thickness

MODEL AND TESTS

The wing tested (reference 7) had an aspect ratio of 8.02, 45° sweepback of the quarter-chord line, taper ratio of 0.45, NACA 63_1A012 airfoil sections, and no geometric twist (fig. 1). The wing was constructed with a solid steel core, and measurements of the twist due to aerodynamic loading showed it to vary linearly with lift coefficient. Under the test conditions of the subject wing, the twist amounted to about 0.2° at $C_L = 1.0$.

Pressure readings were obtained at 225 pressure orifices distributed among 8 stations located at the plane of symmetry and at 3, 10, 30, 55, 75, 90, and 96 percent of the semispan. A typical chordwise distribution of the orifices is shown in figure 1. Further details of the orifice locations and the model can be found in reference 7.

The tests were conducted in the Langley 19-foot pressure tunnel at a Reynolds number of 4.0×10^6, based on the wing mean aerodynamic chord, which, for the tunnel pressure (33 psia) used in these tests,

corresponded to a Mach number of 0.19. Pressure distributions were obtained through the angle-of-attack range from -1° to 30°.

The wing was also tested with two full-chord fences located at 0.575b/2 and 0.800b/2 and one partial-chord fence extending over the aft 65 percent of the chord at 0.890b/2. Similar pressure measurements were made with this configuration except that no pressure data were obtained at 3 percent of the semispan.

REDUCTION AND CORRECTION OF DATA

The pressure coefficients were numerically integrated at each station to obtain section data (lift, drag, and pitching moment). The span loadings indicated that a lift distribution existed at zero lift which flow measurements showed was due mainly to a stream-angle variation in the region occupied by the model. Inasmuch as no satisfactory method for correcting the individual pressure coefficients exists, the experimental basic loading was subtracted from the integrated section data. Further details may be found in reference 7.

No correction was applied to take into account the spanwise variation of the jet-boundary-induced angle since the variation from root to tip was less than 0.2° at a lift coefficient of 1.0. Measurements of the twist of the wing due to deflection under load were found to be roughly of the same magnitude and in the opposite direction. Thus, in addition to being small, the two effects tended to cancel each other. In computing forces and moments from the pressure-distribution data, the following jet-boundary corrections, from reference 8, were applied:

$$\Delta\alpha = 0.387C_L$$

$$\Delta C_D = 0.00634C_L^2$$

$$\Delta C_m = 0.0035C_L$$

These same jet-boundary corrections, and also tare and interference corrections, have been applied to the force-test data. Force-test pitching-moment coefficients have also been corrected for the pitching moment due to the basic loading. Spanwise integration of the section force and moment distributions obtained from the pressure tests resulted in total wing lift, drag, and pitching-moment coefficients.

An indication of the accuracy of the data can be seen in figure 2, where the total wing lift, drag, and pitching-moment coefficients, as determined from both force-test measurements and pressure-distribution

measurements, are plotted. The force-test zero-lift drag coefficient has been added to the drag coefficients determined by pressure measurements in an attempt to partially take into account the friction forces. The agreement of the coefficients determined by the two methods of testing is quite good.

COMPARISON OF EXPERIMENTAL LOADING WITH CALCULATED LOADINGS

In the present section, the experimental loading is compared with loadings calculated by the standard methods proposed by Weissinger, Falkner, and Multhopp, as well as by modifications of these methods. These methods are summarized in table I.

System of Identifying Solutions

All of the methods of calculation recognize the fact that the flow through the wing must be zero, and this condition is fulfilled mathematically at a discrete number of points (called control points). The number and distribution of these points then form a convenient means of identifying solutions. The identification system used in this paper employs two numbers. The first number following the name refers to the number of spanwise stations at which control points are located, while the second number is the number of chordwise control points at each station. For example, Falkner 6 × 3 refers to a Falkner solution utilizing 3 chordwise control points at each of 6 spanwise stations.

Spanwise Load Distribution

As a basis for comparison, the experimental loading at an angle of attack of 4.7° was chosen. Section lift-curve data indicate that at this angle the force characteristics are still linear, and tip separation has not occurred. Practically identical loadings were found at lower angles of attack. For most of the comparisons, data are presented for unit lift coefficient to facilitate the comparisons of the shapes of the spanwise load distributions.

The calculated loadings are compared with the experimental loading in figure 3. These loadings were calculated by using the procedures recommended by the authors. In the Weissinger 7 × 1 solution it is assumed that the circulation is concentrated along the quarter-chord line and that it varies continuously across the span. The downwash is then calculated at 7 spanwise control points on the three-quarter-chord line. No attempt is made to take into account the discontinuity in plan form at the root station. The loading calculated by this method is

too high over the outboard portions. In the Falkner 6 × 3 solution a particular form of a spanwise and a chordwise distribution of circulation is assumed in order to define the strength of a number (21) of discrete horseshoe vortices distributed over the span at each of 6 chordwise locations. The downwash condition is fulfilled at 3 chordwise control points at each of 6 spanwise stations. No attempt is made to take into account the root-station discontinuity. The agreement is fair except at the root stations, where the experimental dip in loading is not predicted. The Multhopp 23 × 1 solution assumes a continuous spanwise and chordwise variation of circulation. The downwash condition is fulfilled at 23 spanwise control points (approximately 3 × aspect ratio). The discontinuity is treated by modifying the geometric characteristics of the wing at the root. Good agreement with experiment is obtained with this method.

All of the calculated loadings differ from one another. The differences are, of course, attributed to the differences in the assumed loading and the control points used to arrive at a solution. To check the influence of the number and location of the spanwise and chordwise control points and the root section discontinuity, the methods were used to calculate the loadings, disregarding some of the authors' recommendations.

Number and location of spanwise control points.- Weissinger states in reference 2 that for straight wings of moderate aspect ratio, 7 control points are all that are necessary for an accurate prediction of the load distribution. Schlichting and Kahlert (reference 9), however, have indicated that if the aspect ratio is increased to infinity, using any finite number of control points will result in a triangularly shaped loading with the minimum at the root. Multhopp states in reference 4 that for accuracy the number of control points should be about three times the aspect ratio. To examine more closely the effect of the number of spanwise control points, several solutions have been carried out in which this parameter was varied. The Weissinger method was carried out using 15 control points and the Multhopp method was carried out using 7 and 15 control points. For each solution, it was necessary to calculate the constants embodied in the simultaneous equations. The number of equations to be solved was equal to the number of control points in a semispan.

Figure 4(a) compares the Weissinger 7 × 1 and 15 × 1 solutions. The 7-point solution predicts too high a loading toward the tip and too low and broad a loading minimum near the root. This type of loading results because the control points (at η = 0, 0.385, 0.707, and 0.923) miss the essential variations in the loading, as can be seen from the experimental data. In addition, the lower-order approximation for the assumed spanwise loading does not involve enough terms to describe accurately the load distribution. Increasing the number of control points

to 15 produces a more accurate loading, since now the spacing of the control points is closer and more terms are used in the assumed loading.

Figure 4(b) compares the experimental data with Multhopp's 7 × 1, 15 × 1, and 23 × 1 solutions. The same logic applies here: The accuracy of the predicted load shape increases as the number of spanwise control points increases.

It was felt that to predict accurately the loading in the neighborhood of the root, it was necessary to locate control points in this region. Since Falkner suggests the opposite view in reference 10, another Falkner solution was carried out, in which only the location of the control points was varied. Figure 5(a) compares the experimental loading with the calculated loadings obtained with the Falkner 6 × 3 solution (control points at η = 0.2, 0.5, and 0.8) and the Falkner 5 × 3 solution (control points at η = 0, 0.5, and 0.8). Without the control point at the center section, the center minimum is not predicted. With the control point at the center section, however, the drop in loading is carried over too far outboard. As previously explained, the effect results from too few control points.

The methods used on unswept wings are such that a majority of the control points are located at the tip sections where the loading varies rapidly. Since a drop in loading is also experienced over the central portions of swept wings, it was felt that a major portion of the increase in accuracy when the number of control points was increased was due to the close spacing of the control points at the root stations. A preliminary study was made to investigate this point more fully by using control points at the plane of symmetry and at 0.1 b/2 intervals outboard along the span. The method of reference 11, which was set up to calculate the downwash resulting from a given loading, was inverted so that the loading required to induce a given downwash could be calculated. This method employs a simplified vortex representation similar to that used by Falkner but does not use the same mathematical techniques and will be referred to as the modified Falkner 19 × 1 method. Twenty-one horseshoe vortices were distributed over the span along the quarter-chord line, as in reference 11, and the downwash was calculated at 19 control points on the three-quarter-chord line. Since the loading is symmetrical, only 10 independent equations, each with 11 unknown loadings, are obtained. The strength of the tip vortex was assumed to be given in terms of the two adjacent vortices by a series of the type $Ax^{1/2} + Bx^{3/2}$, where x is the distance inboard of the tip. The resulting equation

$$\left(\frac{c_l c}{C_L \bar{c}}\right)_{\eta=0.9625} = 0.995\left(\frac{c_l c}{C_L \bar{c}}\right)_{\eta=0.9} - 0.271\left(\frac{c_l c}{C_L \bar{c}}\right)_{\eta=0.8}$$

was substituted into the 10 equations to eliminate one unknown. The equations were then solved for the remaining 10 unknown loadings. No attempt was made to take into account the root section discontinuity. The resulting loading (fig. 5(b)) almost duplicates the experimental loading.

For an accurate prediction of the span loading, it is apparently necessary that the number and location of the control points be such that no essential variation of the loading is missed and that the assumed series for the spanwise loading be of high enough order to fit the loading curve.

Chordwise distribution of control points.- Figure 6 provides a comparison of the experimental loading with that calculated by the Multhopp 15 × 1 and 15 × 2 solutions. It can be seen that the loading is slightly more closely predicted by the Multhopp method when only one chordwise control point is used. The Multhopp method of calculation assumes the wing sections to be mean lines. For the 15 × 1 solution, Multhopp assumes a flat-plate distribution of chordwise circulation, $a_0 \cot \frac{\theta}{2}$. For the 15 × 2 solution, a circular-arc chordwise distribution of circulation, $a_0 \cot \frac{\theta}{2} + a_1 \sin \theta$, is used. The wing investigated was of finite thickness and had a flat mean line, but three-dimensional effects might be expected to induce a camber. The chordwise loading may be represented mathematically by a trigonometric series of the form $a_0 \cot \frac{\theta}{2} + a_1 \sin \theta + a_2 \sin 2\theta + a_3 \sin 3\theta + \ldots$. In order to ascertain the magnitude of the harmonics present in the experimental chordwise loading due to angle of attack, a Fourier analysis was made of each of the chordwise loadings. The analysis showed that the constants for the first three terms (a_0, a_1, and a_2) are significant and of the same order of magnitude, while the coefficients of the higher harmonics are smaller.

A similar analysis, however, was also made for the theoretical loading on a two-dimensional NACA 63_2A015 airfoil section, as given in the $\frac{\Delta v_a}{V}$ tables of reference 12, in order to determine whether the a_1 and a_2 terms might simply be due to the thickness. (The sections of the present wing normal to the leading edge are actually about 16.3 percent thick, but the tables did not give data for this thickness ratio.) The relative values of a_0, a_1, a_2, . . . were found to be very nearly the same as for the wing (except for the root and tip sections). Hence, it is concluded that the relatively large values of a_1 and a_2 found for the wing do not necessarily prove that the 15 × 2 solution

[redacted]

should be intrinsically more exact than the 15 × 1 solution. On the other hand, there would seem to be no very clear reason why the 15 × 2 solution should be less exact. A possible explanation of the lower accuracy of the 15 × 2 solution may be that the forward location of half of the control points gives rise to slight inaccuracies in the mechanics of solution. In reference 9, similar behavior is noted when using the Falkner method with control points located forward on the chord. Effects of viscosity and of finite wing thickness may, of course, also be involved.

Root-section discontinuity.- Experimental investigations on swept wings have shown that the pressure isobars at the root sections are continuously curved rather than sharply bent so that there is no discontinuity in flow. This curving of the pressure isobars at the root produces a flatter chordwise distribution of load with a rearward center of pressure. Both Multhopp (reference 4) and Schlichting and Kahlert (reference 9) recommend that corrective measures be applied at the root sections to take into account this phenomenon. Only the Multhopp method was available for comparison. For the standard solution, Multhopp proposes the use of an equivalent wing which has the same geometry as the actual wing with the exception that the root chord is shortened and shifted rearward in a specified manner so as to round off the apex of the wing. A modified Multhopp solution may be found by neglecting this proposal. In figure 7, the experimental loading is compared with two Multhopp 15 × 1 solutions. The standard solution shows good agreement between theory and experiment. As would be expected, the major effect was at the root stations where the modified solution predicts a lower loading than the standard solution. In general, it appears that the Multhopp correction to take into account the bending of the isobars at the root stations has a small but beneficial effect on the span loading for a wing of this aspect ratio. For wings of smaller aspect ratio, however, the correction may be of greater importance.

Chordwise distribution of circulation.- When the Weissinger 15 × 1 solution is compared with the modified Multhopp 15 × 1 solution (fig. 8), the effect of the chordwise distribution of circulation on the span load distribution can be seen. As previously stated, the Weissinger method assumes the circulation concentrated at the quarter chord, while the Multhopp method assumes a chordwise distribution of the form $a_0 \cot \frac{\theta}{2}$. Both methods compute the downwash at the three-quarter-chord line. The effect of the assumed distribution can be seen to be largest at the root stations where the Multhopp lifting-surface theory predicts a lower loading than the Weissinger second-order lifting-line theory. The total effect appears to be of small importance, and quite possibly, some of the difference may be due to the differences in the computational techniques rather than to differences in the basic methods.

[redacted]

Rapid approximate methods.- The load distributions obtained by two rapid approximate methods are shown in figure 9. The method of reference 5 predicts a load distribution which is in fair agreement with experiment. About 10 minutes was required for a solution.

The loading predicted by the method of reference 6, which is based upon the assumption that wings with similar spanwise centers of pressure have similar load distributions, has been presented for two cases. The first loading was obtained using the center-of-pressure location calculated by the method of reference 6, while the second was obtained using the experimental center-of-pressure location. The first loading is in rather poor agreement with experiment. The second loading is in somewhat better agreement with experiment. Since the method of reference 6 is based upon results obtained by the Weissinger 7 × 1 solution which has been shown to be inadequate for this wing, it is not surprising that corresponding inaccuracies exist. This method is extremely rapid, however, and required less than 5 minutes for each loading.

High lift coefficients.- All of the methods of calculation assume that viscous effects are negligible, that is, that boundary layers are very thin and, in particular, that the flow is unseparated. It is of interest to compare the calculated loadings with the measured loadings at high angles of attack. Figure 10 presents experimental loadings obtained on the wing with fences at three angles of attack. This configuration was used rather than the plain wing because separation occurred at low values of C_L on the plain wing, and, obviously, once the flow separates, the solutions are invalid. The calculated curve presented is the modified Falkner 19 × 1 solution since it predicts the best loading shape at low lift coefficients. At the moderate lift coefficient (0.74), the agreement between the calculated curve and experimental values is still good. At the highest lift coefficient (1.01), the agreement is reasonable although tip stall has begun. It should be noted that the large irregularity at $0.55b/2$ is due to the fact that this station is just inboard of a fence and is apparently in a localized region of separation at both the moderate and high lift coefficients.

Lift-Curve Slope

The experimental lift-curve slope determined for both force and pressure measurements is 0.069 per degree through zero lift. This slope is maintained up to an angle of attack of about 5°, beyond which the slope gradually decreases, as shown in figure 11.

The lift-curve slopes predicted by the various methods of calculation are also indicated in figure 11. The number of spanwise control points utilized had a marked effect on the slope predicted by any one

method. For the Weissinger and Falkner solutions, as the number of spanwise control points is increased, the value of C_{L_α} is increased. However, the opposite is true of the Multhopp method, where an increasing number of control points causes a decrease in lift-curve slope. It appears as if both the Weissinger and Multhopp solutions may be converging toward a common value of C_{L_α} as the number of control points is increased, although there are not enough solutions to examine this point further.

Schlichting and Kahlert, in an analysis of the Mutterperl (reference 13) and Weissinger (reference 2) methods, conclude that by not locating a control point at the center section a higher lift-curve slope will result. A comparison of the Falkner 6 × 3 and 5 × 3 solutions appears to verify this conclusion. Each solution uses 3 control points in a semispan and an equal number of terms in the approximation for the assumed span loading. A marked decrease in C_{L_α} results partially from locating a control point at the plane of symmetry and partially from decreasing the number of spanwise control points. It would seem, then, that the close agreement between the Falkner 6 × 3 solution and experiment, with regard to C_{L_α}, depends to a large extent upon the particular choice of control-point location.

Reference 9 also points out that in order for C_{L_α} to reach the correct value when a control point is located at the center section, special treatment must be given to the center section to take into account the discontinuity in plan form. When the Multhopp 15 × 1 standard solution, where the center section is rounded, is compared with the Multhopp 15 × 1 modified solution, the increase is evident. The addition of a corrective term at the plane of symmetry increases C_{L_α}. In this instance the increase was only 1.3 percent of the experimental value, which is of the same order of magnitude as reported in reference 8.

All of the methods of calculation (which are based on thin-airfoil theory) underestimate C_{L_α}, and those methods which result in a fairly accurate load shape underestimate C_{L_α} by about 8 percent. This difference is presumably due to the finite thickness of the airfoil and is, in fact, equal to the difference found experimentally between the two-dimensional lift-curve slope for NACA 63-series airfoil sections of about this thickness ratio (about 16.2 percent normal to the leading edge) and the slope given by two-dimensional thin-airfoil theory (see reference 12). The theoretical value of C_{L_α} for these thick sections exceeds that for thin airfoils by about 12 percent.

[redacted]

Center of Pressure

The spanwise position of the center of pressure (fig. 12) is predicted with the greatest accuracy by the methods that most accurately predict the spanwise load distribution. Obviously, then, what has previously been said about an accurate prediction of load shape applies here: The number and location of the control points has the largest influence on the prediction of the spanwise center of pressure.

The chordwise position of the center of pressure is also shown in figure 12. Except for the Falkner solutions and the Multhopp 15 × 2 solution, the chordwise location of the center of pressure has been assumed to be on the quarter-chord line for lack of anything better. This assumption is equivalent to assuming that the section acts as a flat plate and that the higher harmonics are zero. For the Falkner and Multhopp 15 × 2 solutions, the wing center of pressure is not necessarily at the quarter-chord line of the wing. For this wing, however, the calculations (neglecting the unknown second harmonic in the Multhopp solution) showed the chordwise center of pressure to be essentially on the quarter-chord line.

The spanwise variations of the local center of pressure predicted by the Falkner 6 × 3 and 5 × 3 solutions and the Multhopp 15 × 2 solution are shown in figure 13. For comparison, the experimental data for four angles of attack for both the plain wing and the wing with fences are shown as unconnected symbols. The lower angle of attack (2.7°) is representative of the low angle range. It can be seen that as the angle of attack is increased for the plain wing, tip stall causes the local centers of pressure to move rearward. With fences, this movement is somewhat retarded until the wing stalls ($\alpha = 21.0°$). It is interesting to note that at $\alpha = 17.0°$ $\left(C_L = 1.01\right)$, the shape of the spanwise loading curve for the fenced wing is still very similar to the curves for the lower angles of attack as shown in figure 10, despite the fact that a considerable rearward movement of the local centers of pressure is shown in figure 13. The values calculated by the Multhopp 15 × 2 method are in good agreement with experiment, predicting the rearward locations at the root and the forward locations at the tip. The standard Falkner 6 × 3 solution is only in fair agreement with experiment, and it can be seen that without special handling (such as given in reference 9) at the root section, the rearward shift of the centers of pressure is not predicted. The Falkner 5 × 3 solution predicts the center of pressure too far rearward over the inboard portions of the wing and too far forward over the outboard portions of the span.

Wing Pitching Moment

It is of interest to apply the previously mentioned parameters to the prediction of the over-all wing characteristics. In figure 14 is plotted the experimental pitching-moment coefficient against lift coefficient for the plain wing and the wing with fences, as well as various calculated curves. The pitching moment due to lift is a function of the center-of-pressure location; thus good agreement is obtained for the more accurate loading methods. It is interesting to note that the spread of the curves represents a center-of-pressure variation of about 12 percent mean aerodynamic chord. The Multhopp 15 × 2 solution practically coincides with the experimental data obtained with fences on.

Induced Drag

The calculated variation of induced-drag coefficient with lift coefficient is shown in figure 15. Most of the calculated curves fall in a narrow band with about a 5-percent spread. These calculations are dependent upon both the lift-curve slope and the load distribution, and it appears as if any reasonable estimate of these characteristics will predict the induced drag fairly well. The load shape resulting from the Falkner 5 × 3 solution combined with the low C_{L_α}, however, predicts an induced-drag coefficient about 30 percent higher than those predicted by the other solutions.

CONCLUDING REMARKS

Experimental force and moment data obtained by pressure measurements on a wing of aspect ratio 8.02, 45° sweepback of the quarter-chord line, taper ratio of 0.45, and NACA 63_1A012 airfoil sections have been compared with the calculated loadings obtained by the standard methods of Weissinger, Falkner, and Multhopp.

1. With regard to the shape of the spanwise loading distribution, the most accurate load shape was predicted by the Multhopp 23 × 1 solution. The standard Falkner 6 × 3 solution did not predict the experimental drop in loading at the root stations.

2. All of the methods predicted similar load shapes provided that a sufficient number of spanwise control points were used in the solution. At least 15 were necessary for this wing.

[redacted]

3. It was found that a slight improvement in lift-curve slope and loading shape resulted when the Multhopp scheme of rounding the apex of the wing was used.

4. Although the opposite effect was expected, it was found that the Multhopp method using 1 chordwise control point predicted a more accurate loading than that using 2 chordwise control points.

5. Those methods which predicted the loading shape fairly accurately predicted the lift-curve slope about 8 percent too low. The low estimate is probably caused by the finite thickness of the wing.

6. The spanwise variation of the chordwise position of the center of pressure was fairly accurately predicted by the Multhopp method with 2 chordwise control points.

7. It appears as if the Multhopp or the Weissinger method will result in the best over-all compromise between lift-curve slope and load shape, provided enough control points are used in the solution. For an extremely rapid estimate of the load shape, Diederich's method predicted a reasonably accurate loading for this wing.

Langley Aeronautical Laboratory
National Advisory Committee for Aeronautics
Langley Field, Va.

[redacted]

REFERENCES

1. Van Dorn, Nicholas H., and DeYoung, John: A Comparison of Three Theoretical Methods of Calculating Span Load Distribution on Swept Wings. NACA TN 1476, 1947.

2. Weissinger, J.: The Lift Distribution of Swept-Back Wings. NACA TM 1120, 1947.

3. Falkner, V. M.: The Calculation of Aerodynamic Loading on Surfaces of Any Shape. R. & M. No. 1910, British A.R.C., 1943.

4. Multhopp, H.: Methods for Calculating the Lift Distribution of Wings (Subsonic Lifting Surface Theory). Rep. No. Aero 2353, British R.A.E., Jan. 1950.

5. Diederich, Franklin W.: A Simple Approximate Method for Obtaining Spanwise Lift Distributions over Swept Wings. NACA RM L7I07, 1948.

6. Jones, R. Stanton: An Empirical Method for Rapidly Determining the Loading Distributions on Swept Back Wings. Rep. No. 32, College of Aero., Cranfield (British), Jan. 1950.

7. Graham, Robert R.: Low-Speed Characteristics of a 45° Sweptback Wing of Aspect Ratio 8 from Pressure Distributions and Force Tests at Reynolds Numbers from 1,500,000 to 4,800,000. NACA RM L51H13, 1951.

8. Sivells, James C., and Salmi, Rachel M.: Jet-Boundary Corrections for Complete and Semispan Swept Wings in Closed Circular Wind Tunnels. NACA TN 2454, 1951.

9. Schlichting, H., and Kahlert, W.: On the Calculation of the Lift Distribution of Swept Wings. Rep. No. Aero. 2297, British R.A.E., Oct. 1948.

10. Falkner, V. M.: The Solution of Lifting Plane Problems by Vortex Lattice Theory. Rep. No. 10,895, British A.R.C., Sept. 29, 1947.

11. Diederich, Franklin W.: Charts and Tables for Use in Calculations of Downwash of Wings of Arbitrary Plan Form. NACA TN 2353, 1951.

12. Abbott, Ira H., Von Doenhoff, Albert E., and Stivers, Louis S., Jr.: Summary of Airfoil Data. NACA Rep. 824, 1945. (Formerly NACA ACR L5C05.)

13. Mutterperl, William: The Calculation of Span Load Distributions on Swept-Back Wings. NACA TN 834, 1941.

[redacted]

TABLE I.- COMPARISON OF METHODS OF CALCULATING LOAD DISTRIBUTION

Method	Spanwise location of control points	Chordwise location of control points	Treatment of root section	Chordwise distribution of vorticity
Weissinger:				
7 × 1	0, 0.3827, 0.7071, 0.9239	$\frac{3c}{4}$	None	Concentrated at $\frac{c}{4}$
15 × 1	0, 0.1951, 0.3827, 0.5556, 0.7071, 0.8315, 0.9239, 0.9808	$\frac{3c}{4}$	None	Concentrated at $\frac{c}{4}$
Falkner:				
6 × 3	0.2, 0.5, 0.8	$\frac{15c}{24}$, $\frac{19c}{24}$, $\frac{23c}{24}$	None	Concentrated at $\frac{c}{24}$, $\frac{5c}{24}$, $\frac{9c}{24}$, $\frac{13c}{24}$, $\frac{17c}{24}$, $\frac{21c}{24}$
5 × 3	0, 0.5, 0.8	$\frac{15c}{24}$, $\frac{19c}{24}$, $\frac{23c}{24}$	None	Concentrated at $\frac{c}{24}$, $\frac{5c}{24}$, $\frac{9c}{24}$, $\frac{13c}{24}$, $\frac{17c}{24}$, $\frac{21c}{24}$
19 × 1 (Modified)	0, 0.1, 0.2, 0.3, 0.4, 0.5, 0.6, 0.7, 0.8, 0.9	$\frac{3c}{4}$	None	Concentrated at $\frac{c}{4}$
Multhopp:				
7 × 1	0, 0.3827, 0.7071, 0.9239	$\frac{3c}{4}$	Bent root station	Distributed over chord $\left(a_0 \cot \frac{\theta}{2}\right)$
15 × 1	0, 0.1951, 0.3827, 0.5556, 0.7071, 0.8315, 0.9239, 0.9808	$\frac{3c}{4}$	Bent root station	Distributed over chord $\left(a_0 \cot \frac{\theta}{2}\right)$
15 × 1 (Modified)	0, 0.1951, 0.3827, 0.5556, 0.7071, 0.8315, 0.9239, 0.9808	$\frac{3c}{4}$	None	Distributed over chord $\left(a_0 \cot \frac{\theta}{2}\right)$
23 × 1	0, 0.1305, 0.2588, 0.3827, 0.500, 0.6088, 0.7071, 0.7934, 0.8660, 0.9239, 0.9659, 0.9914	$\frac{3c}{4}$	Bent root station	Distributed over chord $\left(a_0 \cot \frac{\theta}{2}\right)$
15 × 2	0, 0.1951, 0.3827, 0.5556, 0.7071, 0.8315, 0.9239, 0.9808	0.3455c and 0.9045c	Bent root station	Distributed over chord $\left(a_0 \cot \frac{\theta}{2} + a_1 \sin \theta\right)$

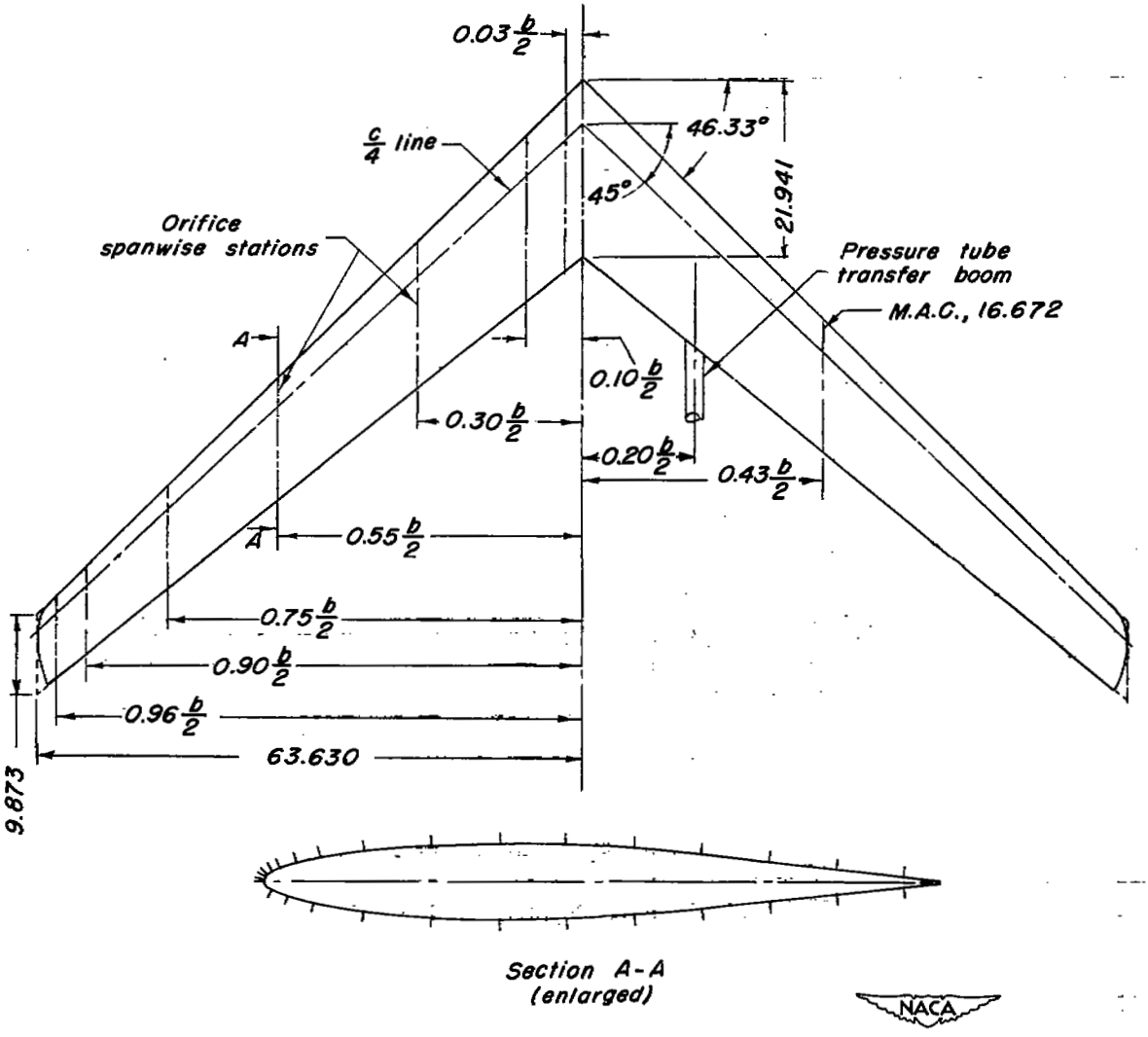

Typical chordwise orifice locations

Figure 1.- Geometric characteristics of model. Aspect ratio, 8.02; taper ratio, 0.45; airfoil section, NACA 63_1A012. (Dimensions in inches except as noted.)

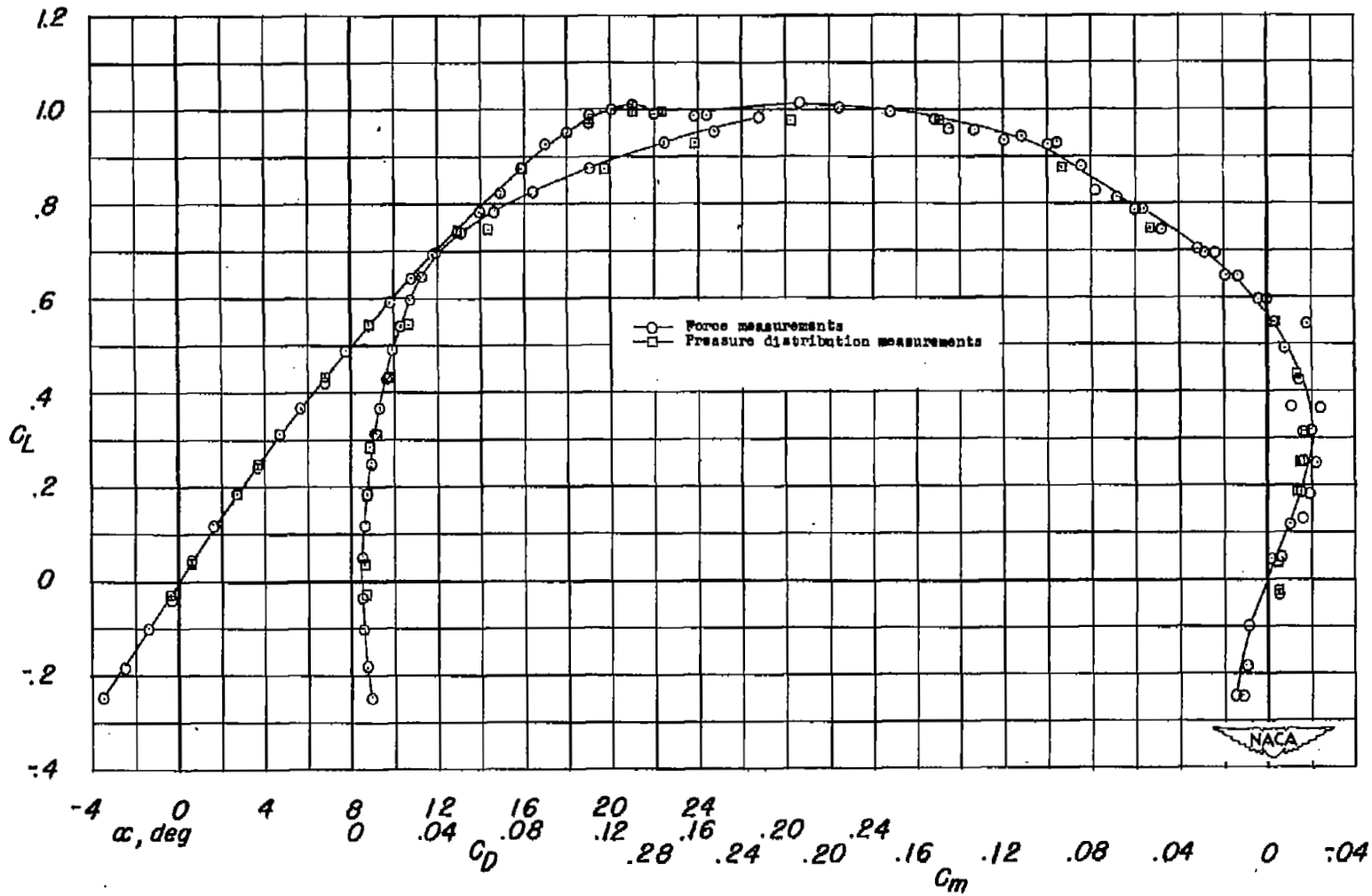

Figure 2.- Variation of lift coefficient with angle of attack, drag coefficient, and pitching-moment coefficient obtained by total-force measurements and pressure measurements.

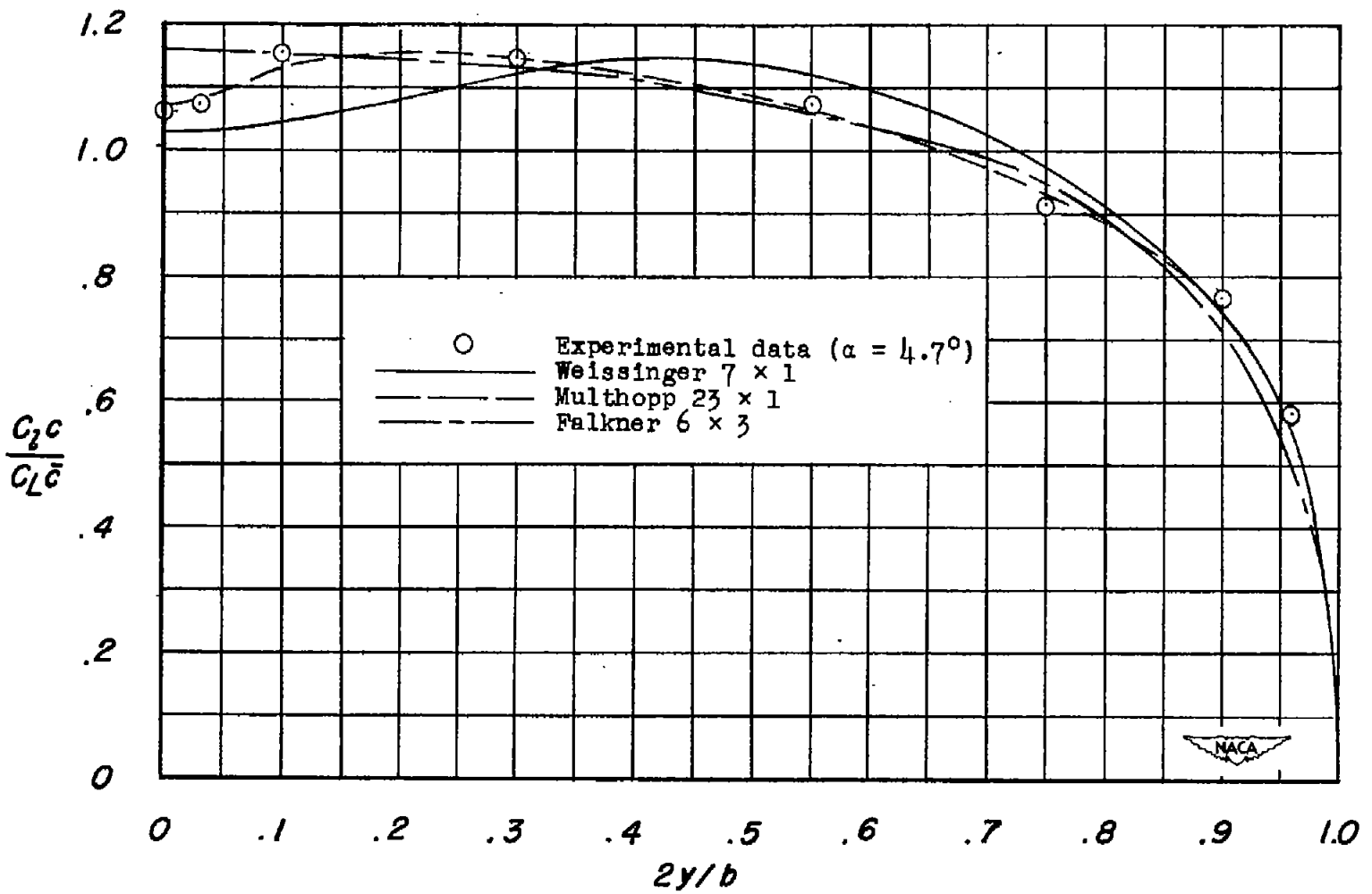

Figure 3.- Experimental span load distribution compared with span load distributions calculated by several standard procedures.

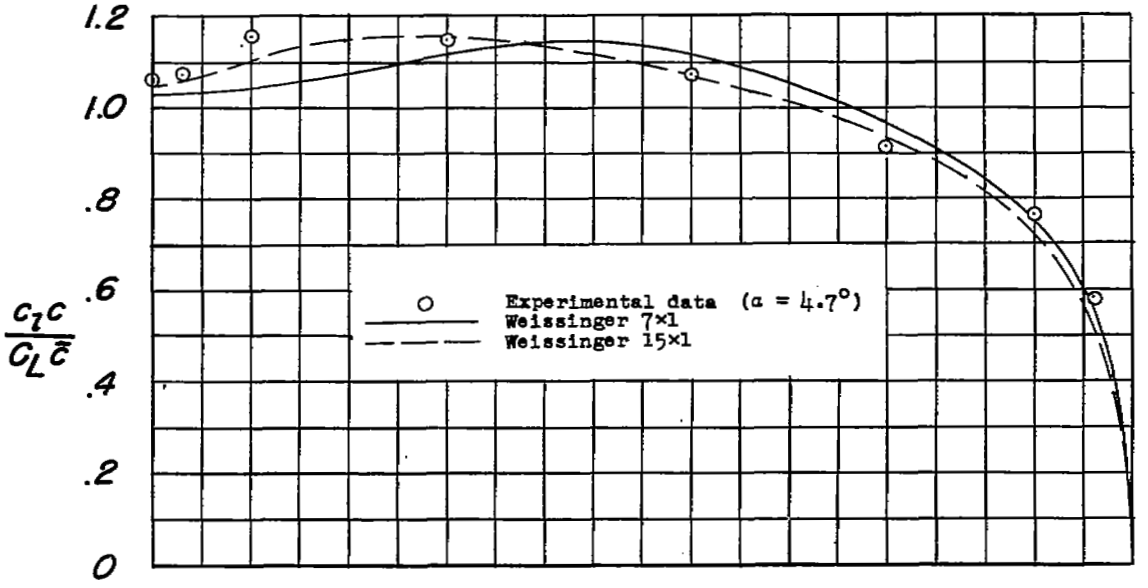

(a) Weissinger method.

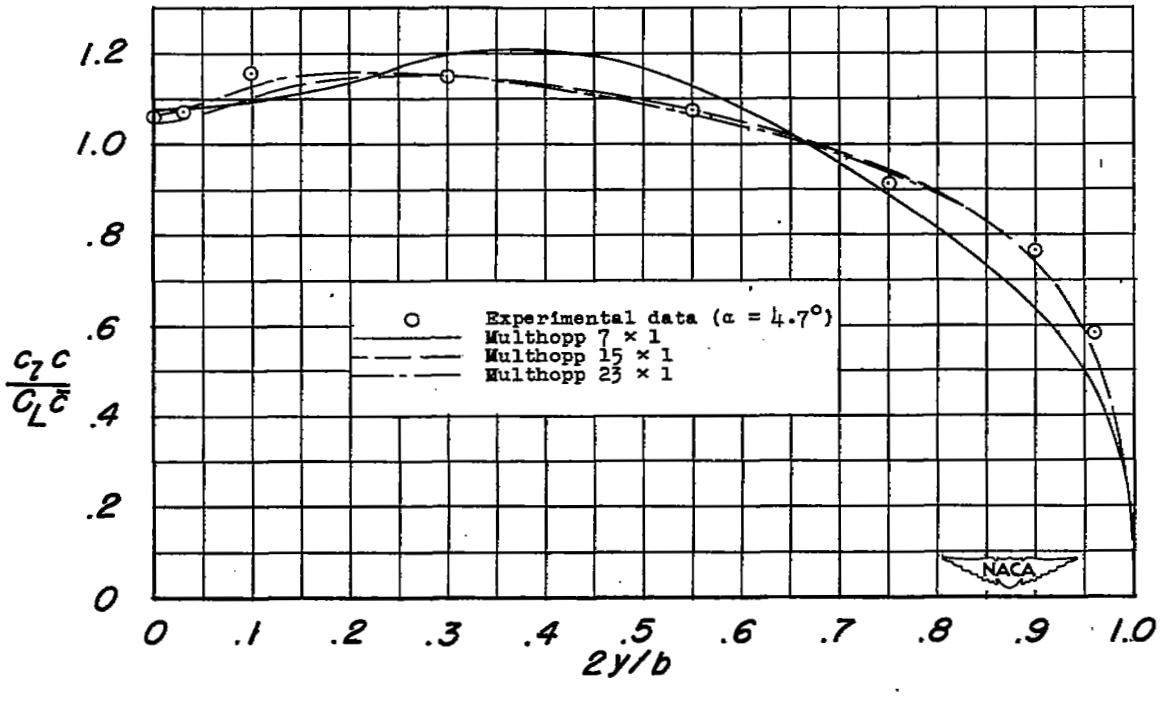

(b) Multhopp method.

Figure 4.- Effect of number of spanwise control points on the span load distribution.

[redacted]

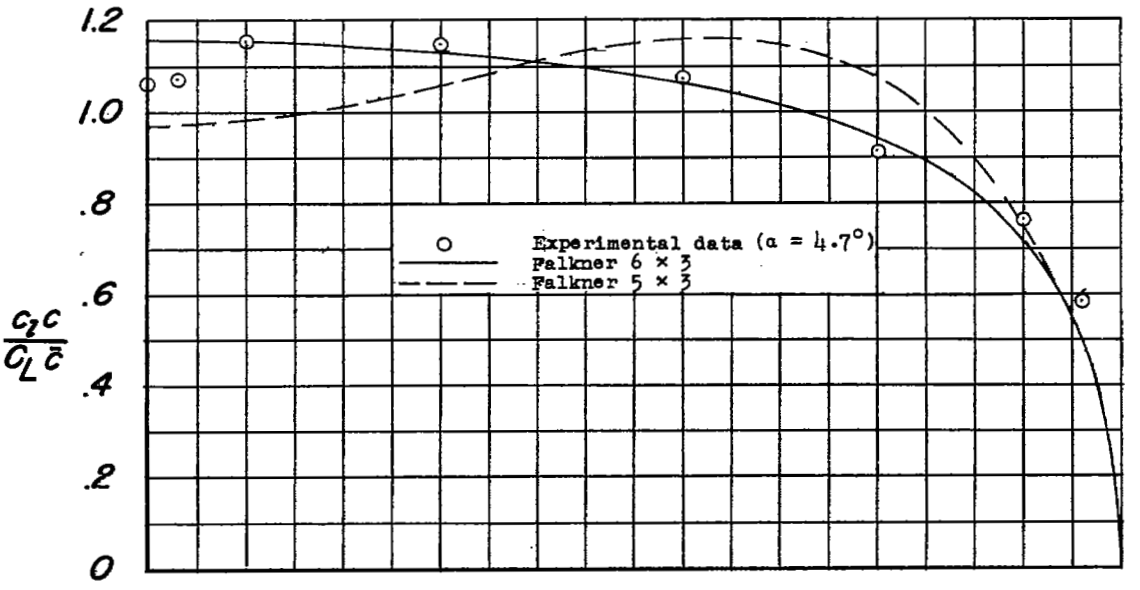

(a) Falkner method.

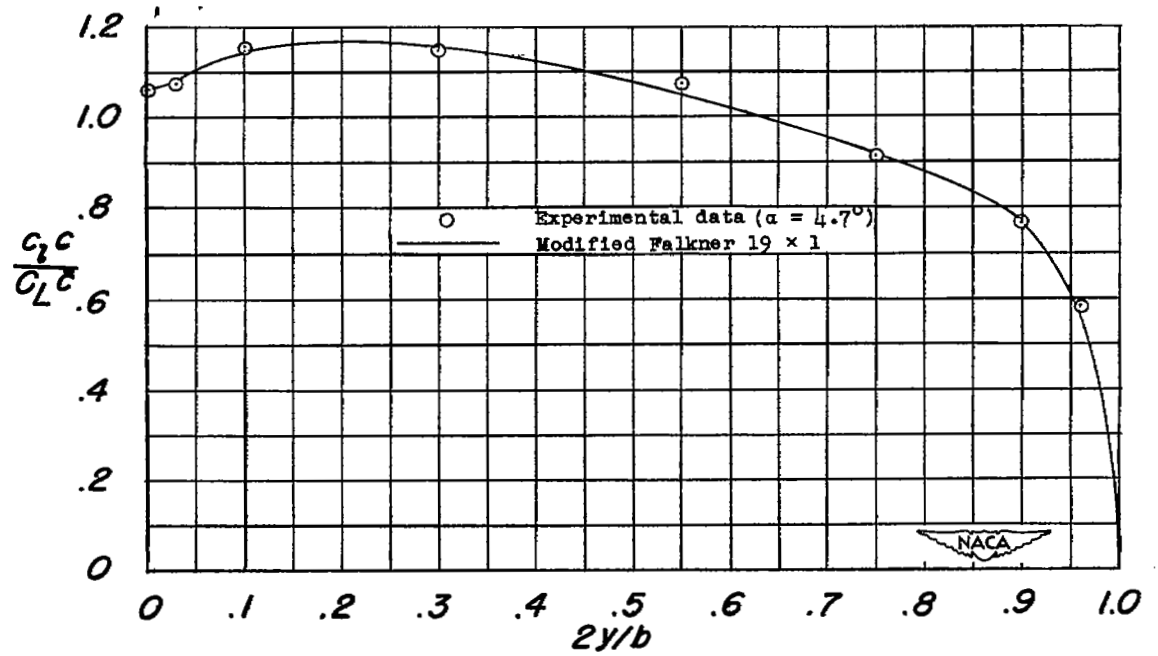

(b) Modified Falkner method.

Figure 5.- Effect of location and number of spanwise control points on the span load distribution.

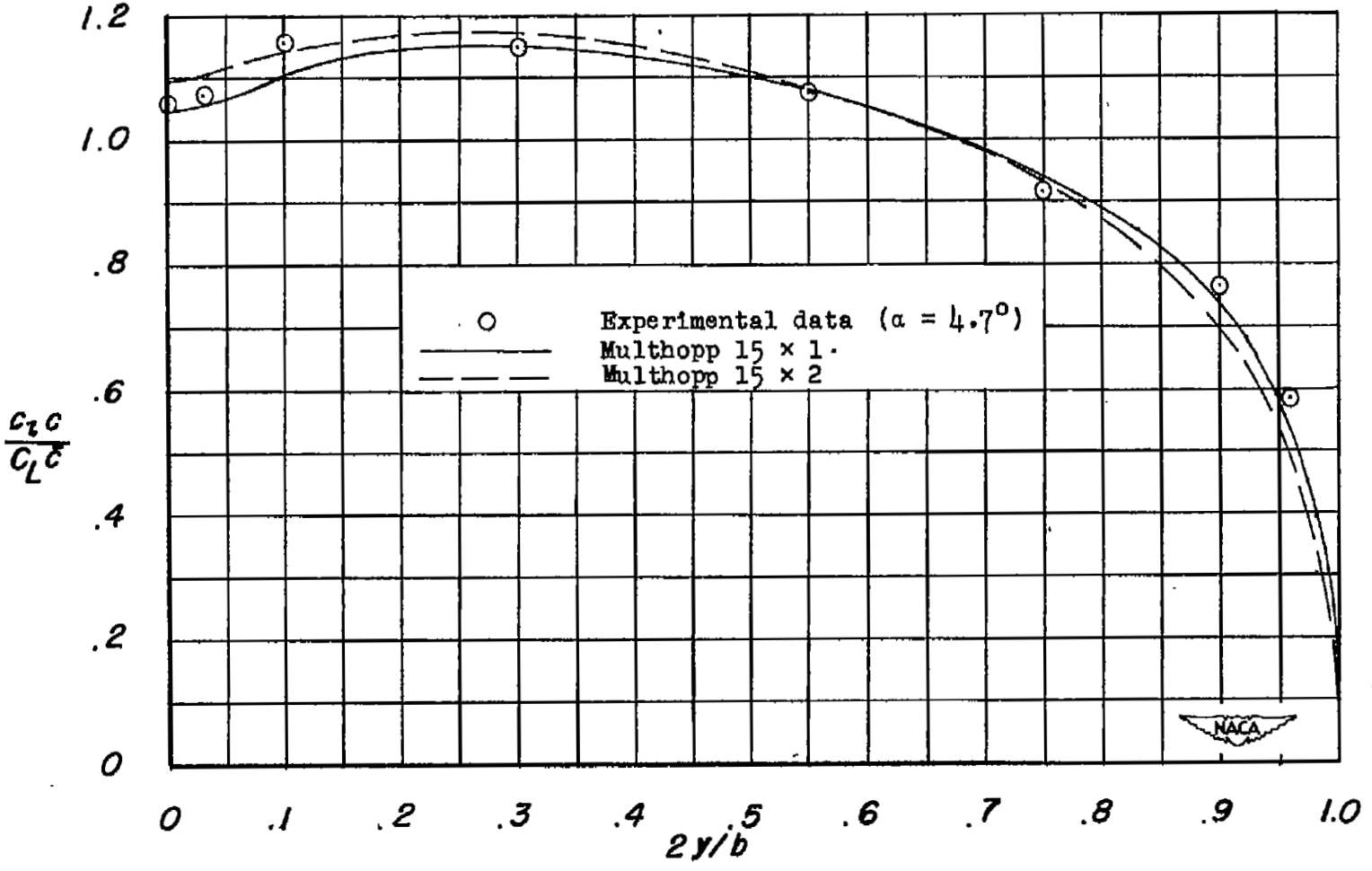

Figure 6.- Effect of chordwise number of control points on span load distribution.

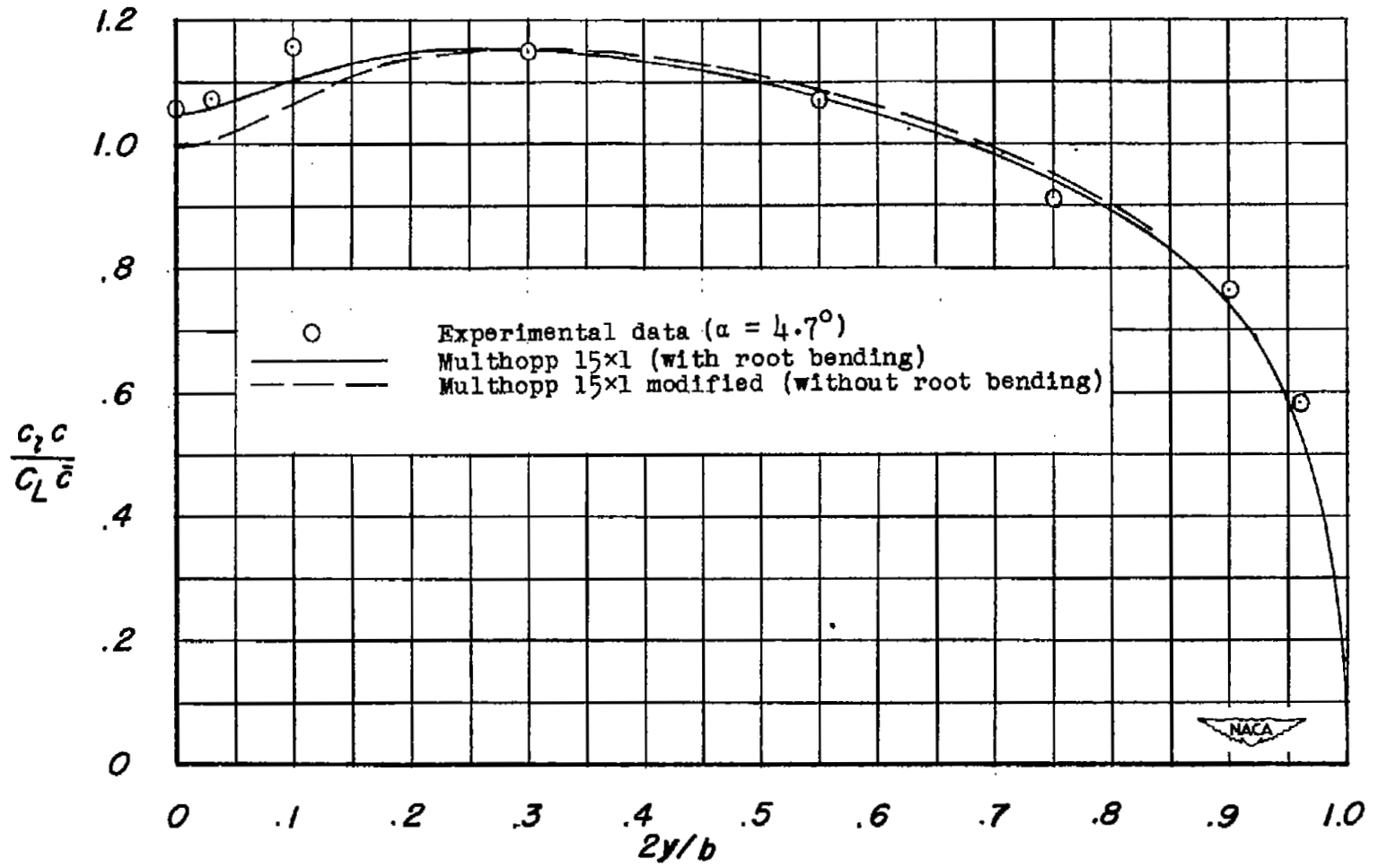

Figure 7.- Effect of the Multhopp bending at the root stations on the span load distribution.

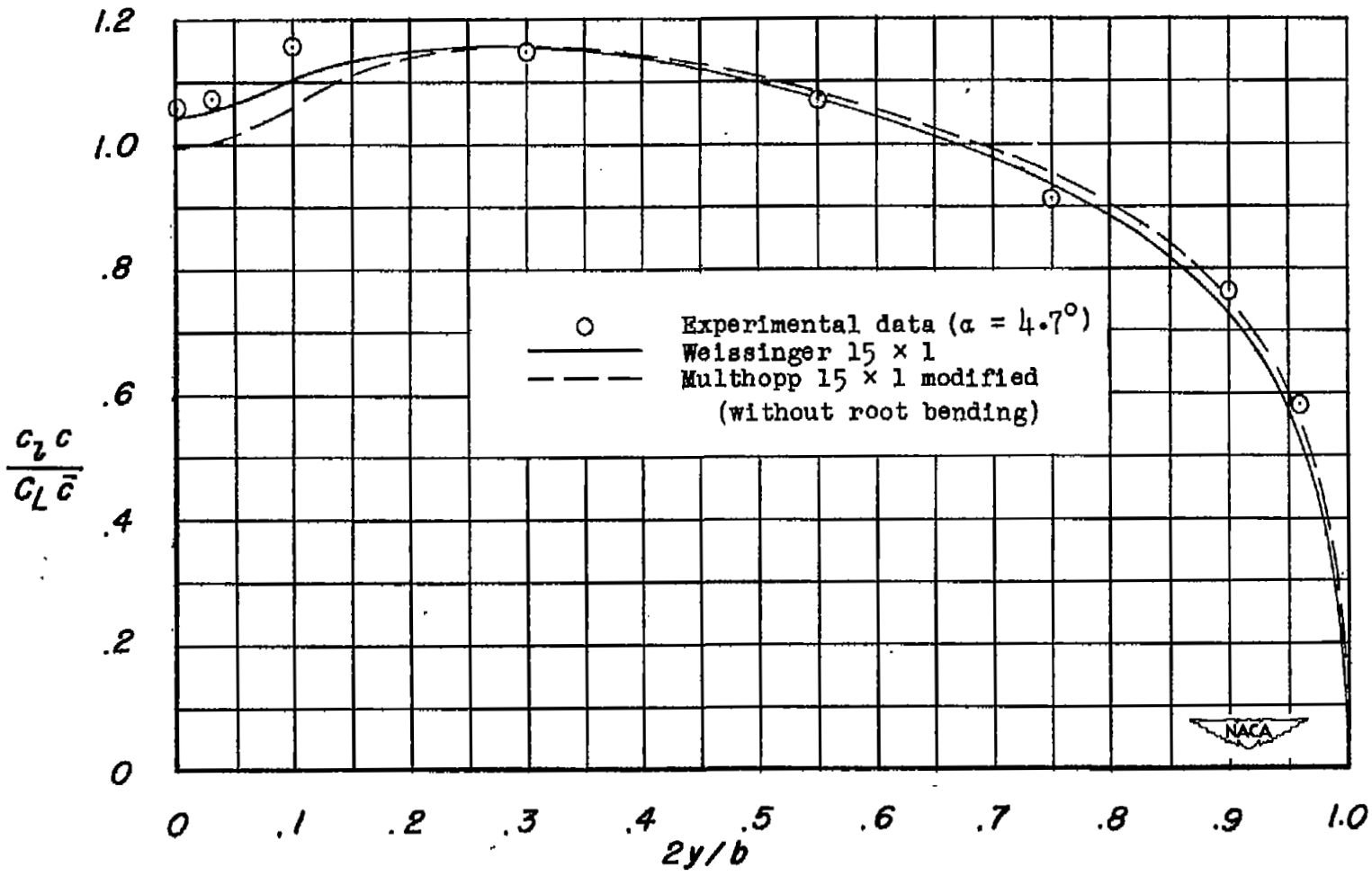

Figure 8.- Effect of an assumed chordwise circulation distribution.

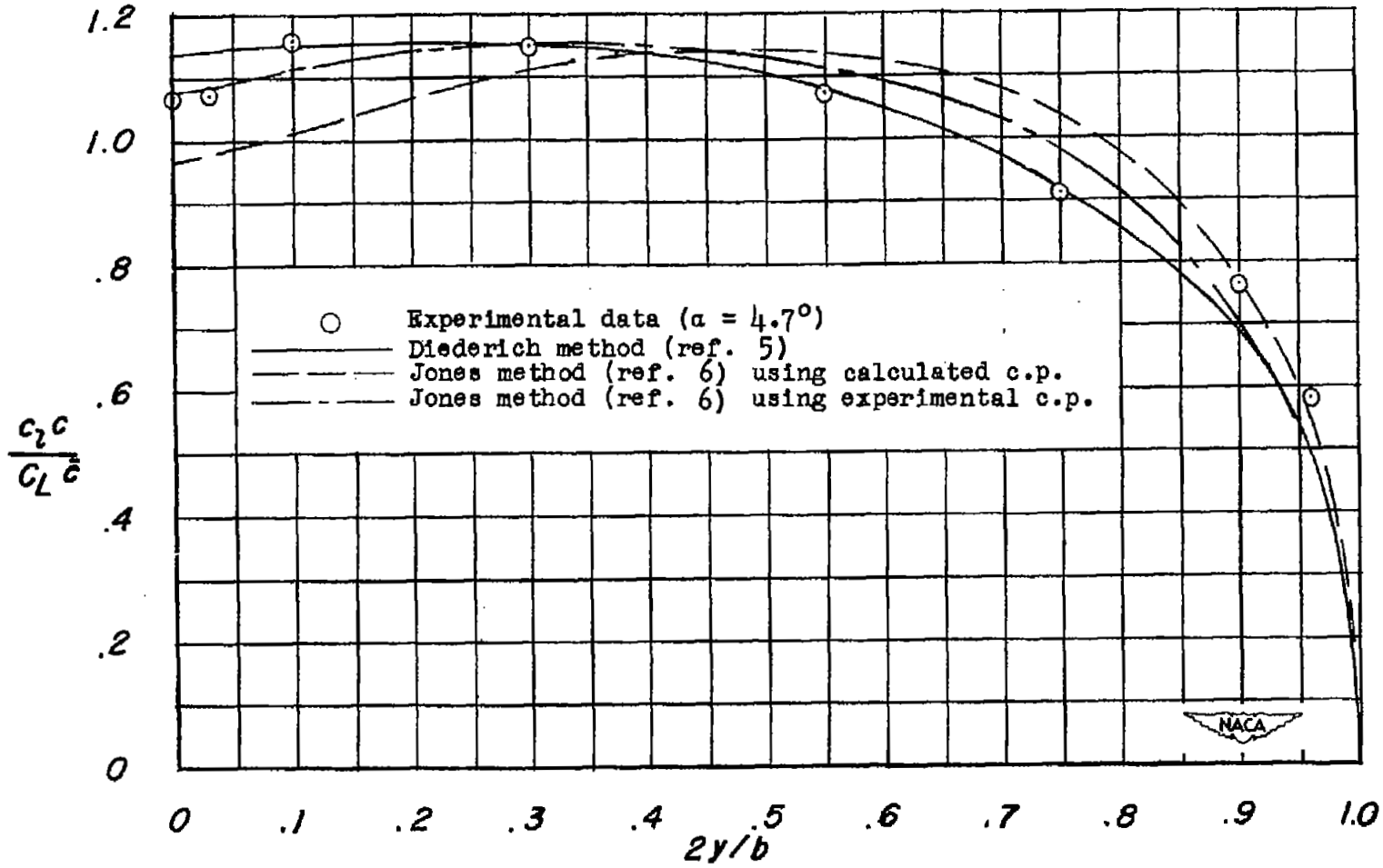

Figure 9.- Comparison of span load distributions obtained by rapid approximate methods.

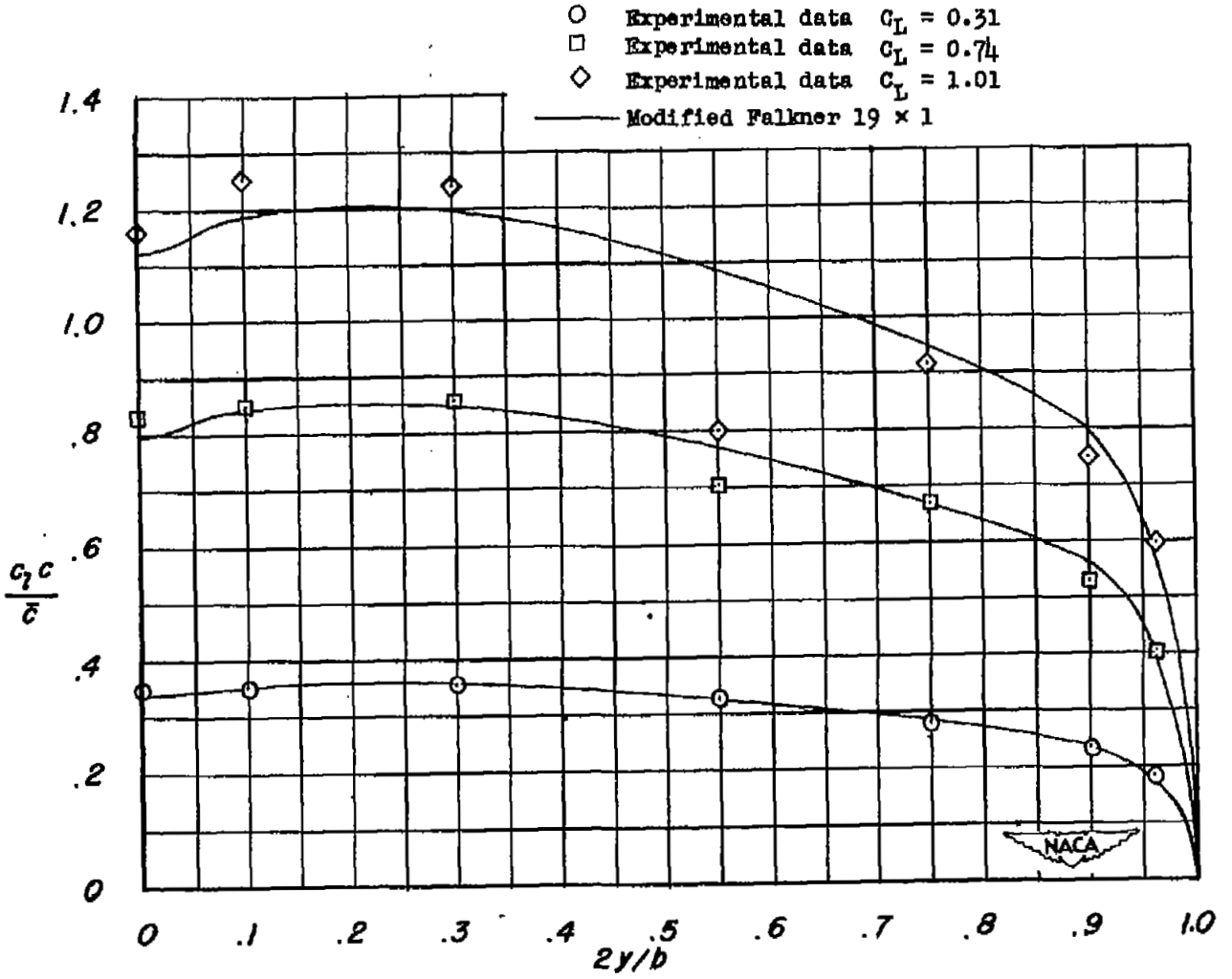

Figure 10.- Calculated and experimental span load distribution at several values of lift coefficients for the wing equipped with fences.

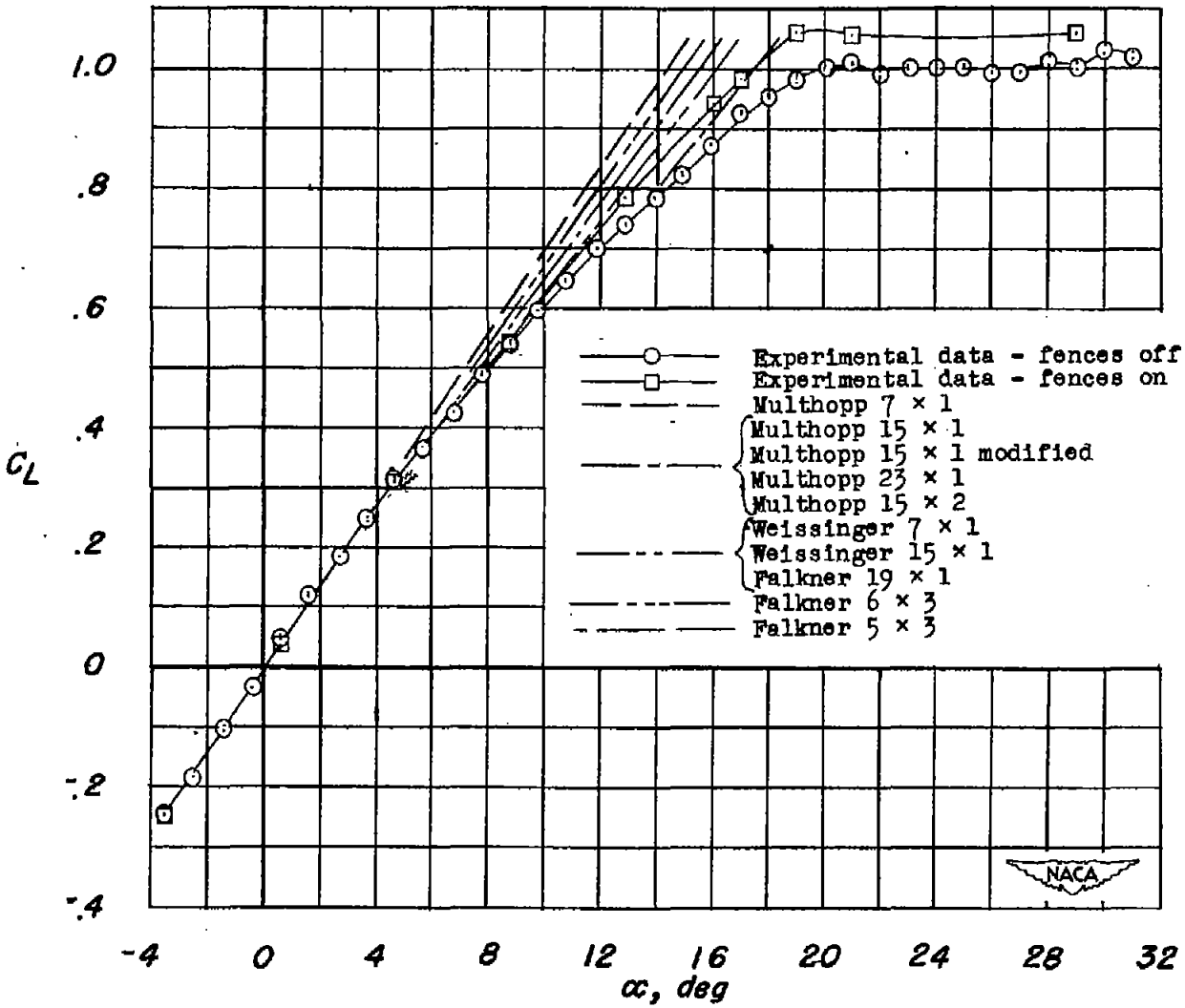

$\frac{dC_L}{d\alpha}$
0.069
.069
.0686
.0649
.0640
.0639
.0650
.062
.0635
.062
.067
.0573

Figure 11.- Comparison of experimental lift-curve slope with calculated values.

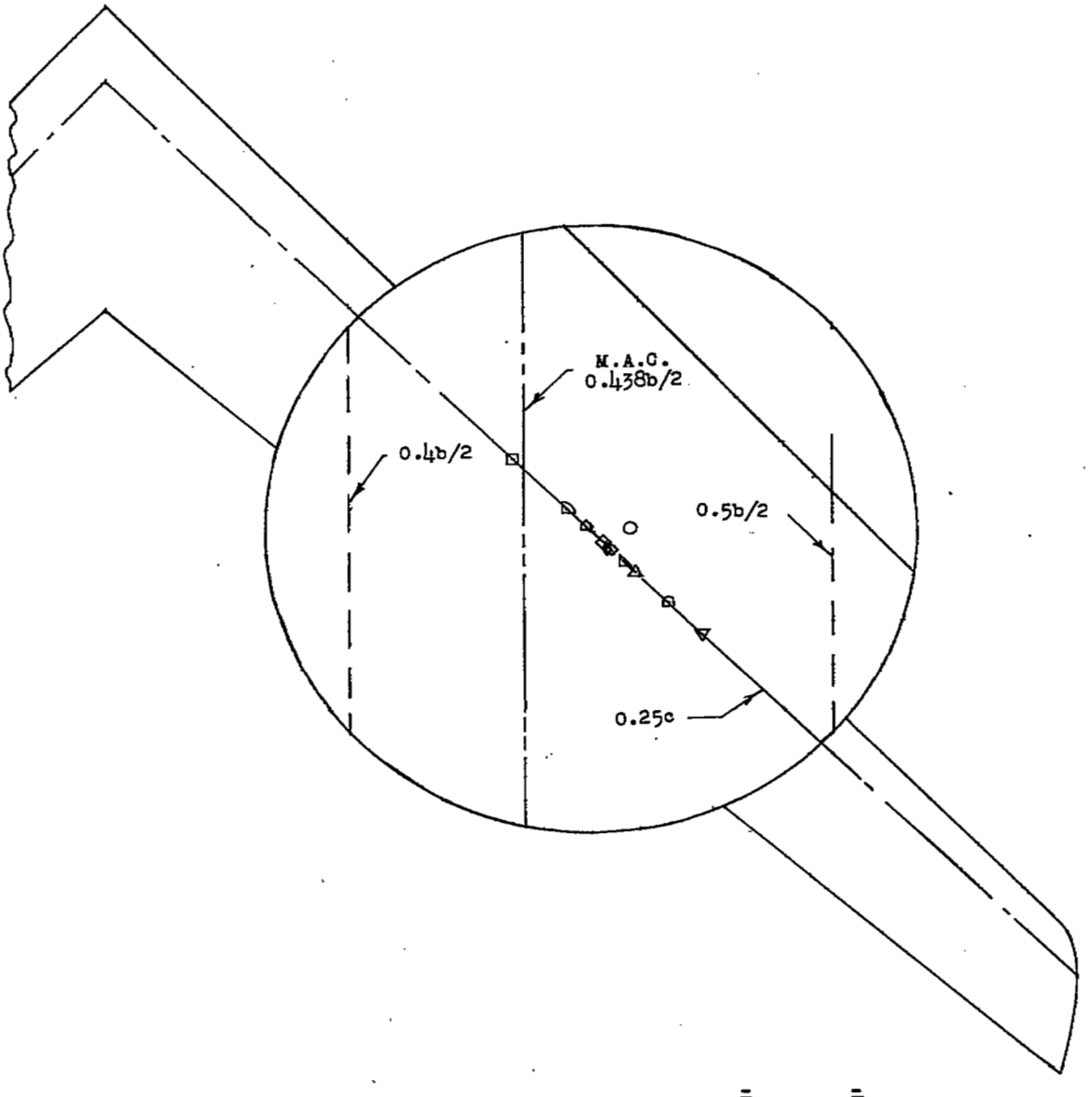

		$\bar{x}$	$\bar{y}$
○	Experiment $\alpha = 4.7°$	0.328	0.458
□	Multhopp 7 × 1	.244	.434
◇	Multhopp 15 × 1	.320	.455
△	Multhopp 15 × 1 modified	.339	.459
⊿	Multhopp 23 × 1	.331	.457
⧠	Multhopp 15 × 2	.282	.445
⧈	Weissinger 7 × 1	.363	.466
◈	Weissinger 15 × 1	.316	.454
◊	Falkner 21 × 1	.313	.453
⌓	Falkner 6 × 3	.297	.449
▽	Falkner 5 × 3	.390	.473

Figure 12.- Location of experimental and calculated center of pressure.

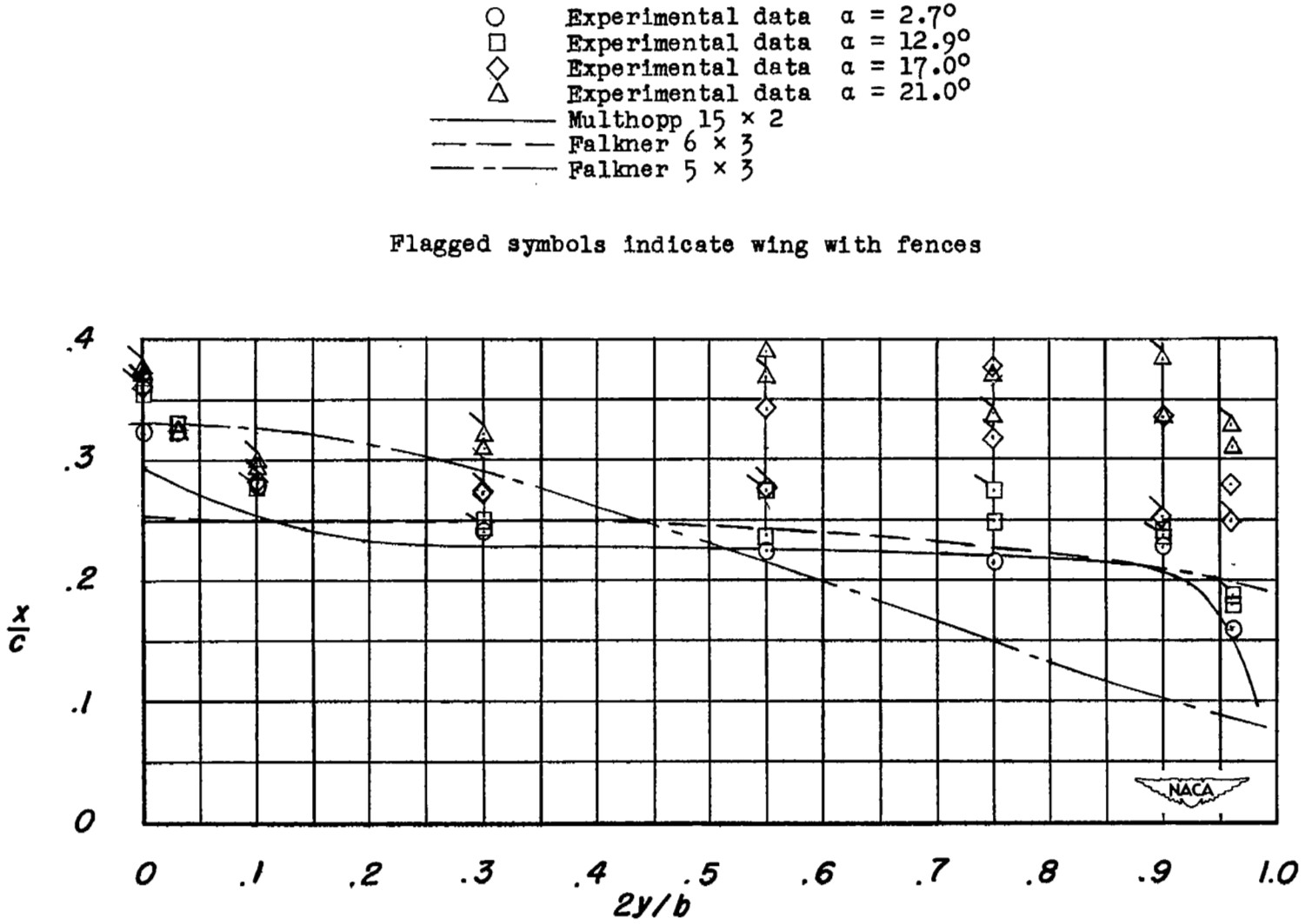

Figure 13.- Calculated and experimental chordwise location of the local center of pressure across the span.

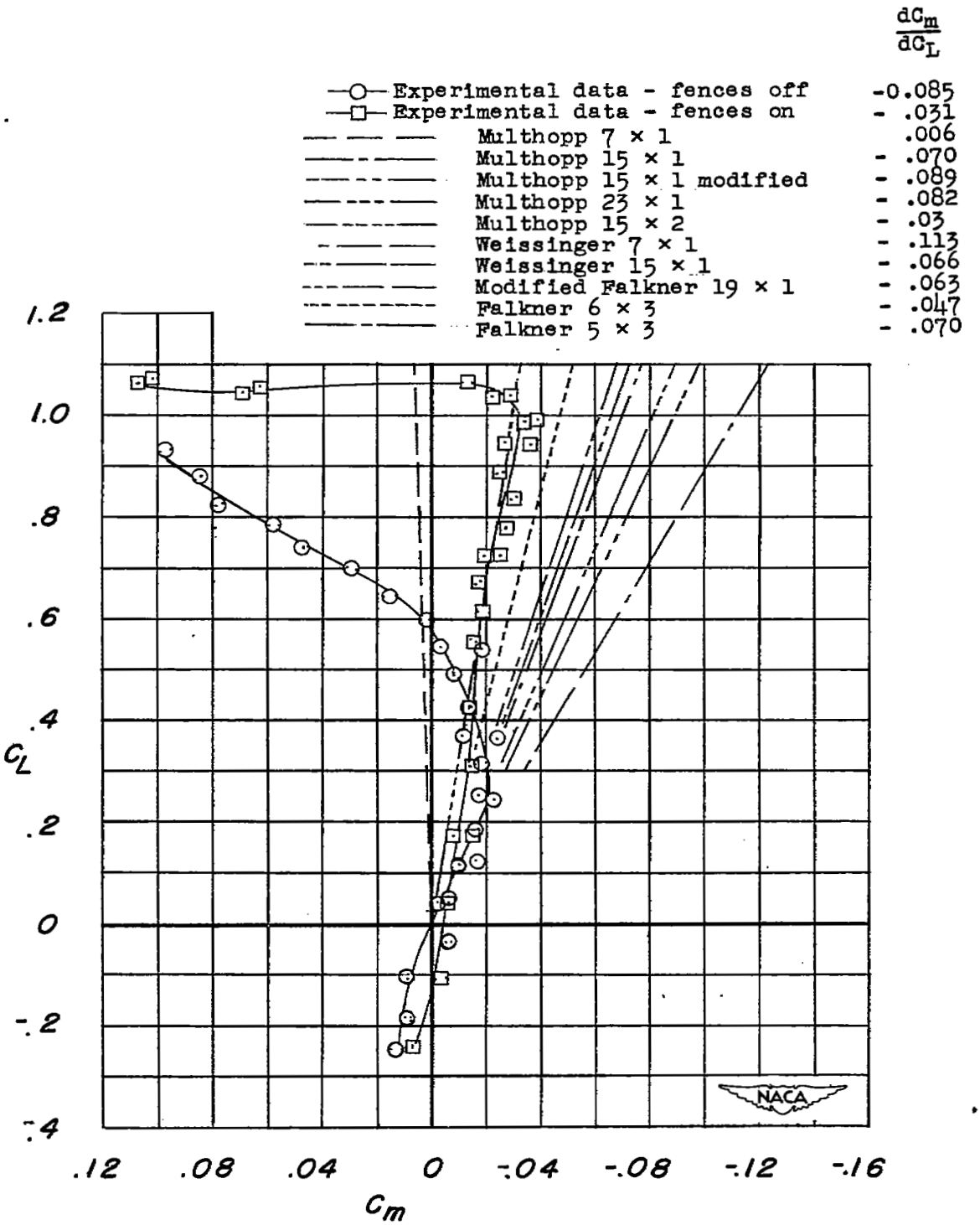

Figure 14.- Calculation and experimental variation of pitching-moment coefficient with lift coefficient.

[redacted]

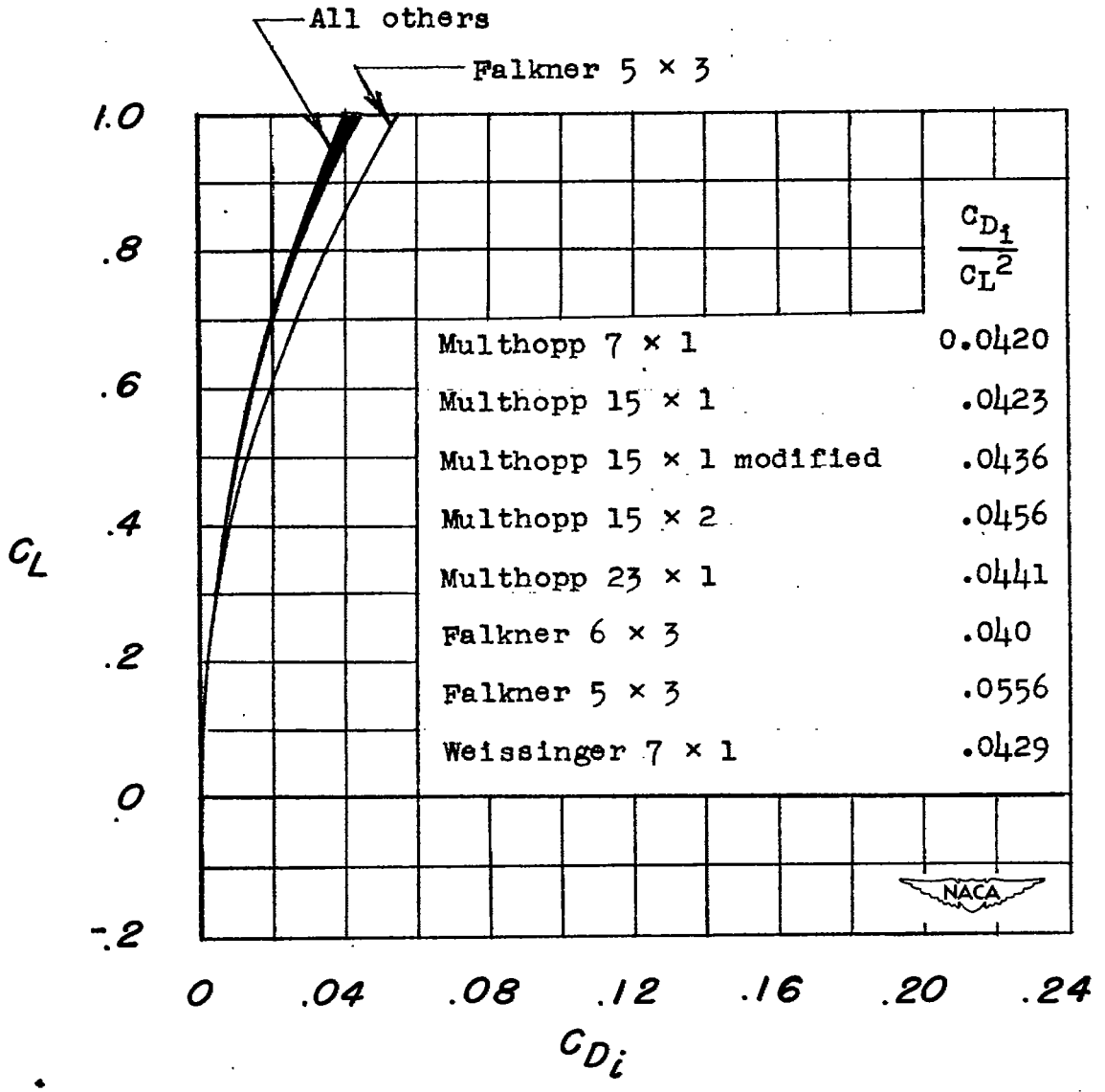

Figure 15.- Calculated variation of induced-drag coefficient with lift coefficient.

NACA-Langley - 1-29-52 - 325